



HAL
open science

Se(VI) sorption from aqueous solution using alginate/polyethylenimine membranes: Sorption performance and mechanism

Yayuan Mo, Thierry Vincent, Catherine Faur, Eric Guibal

► **To cite this version:**

Yayuan Mo, Thierry Vincent, Catherine Faur, Eric Guibal. Se(VI) sorption from aqueous solution using alginate/polyethylenimine membranes: Sorption performance and mechanism. *International Journal of Biological Macromolecules*, 2020, 147, pp.832-843. 10.1016/j.ijbiomac.2019.10.055 . hal-02456526

HAL Id: hal-02456526

<https://imt-mines-ales.hal.science/hal-02456526>

Submitted on 17 Mar 2020

HAL is a multi-disciplinary open access archive for the deposit and dissemination of scientific research documents, whether they are published or not. The documents may come from teaching and research institutions in France or abroad, or from public or private research centers.

L'archive ouverte pluridisciplinaire **HAL**, est destinée au dépôt et à la diffusion de documents scientifiques de niveau recherche, publiés ou non, émanant des établissements d'enseignement et de recherche français ou étrangers, des laboratoires publics ou privés.

Se(VI) sorption from aqueous solution using alginate/polyethylenimine membranes: Sorption performance and mechanism

Yayuan Mo^a, Thierry Vincent^a, Catherine Faur^b, Eric Guibal^{a,*}

^a C2MA, IMT Mines Ales, Ales, France

^b IEM, Institut Européen des Membranes, Univ Montpellier, CNRS, ENSCM, Montpellier, France

ABSTRACT

New high percolating alginate membranes are designed without using sophisticated drying methods: negatively charged alginate reacts with positively charged polyethylenimine (PEI), prior to be crosslinked with glutaraldehyde and air-dried. This is sufficient to obtain a highly macroporous structured membrane. Highly percolating properties of these new A-PEI membranes make the material applicable in natural drainage systems. The high density of amine groups in composite membranes explain their high affinity for anions in acidic solutions. FTIR, SEM-EDX and XPS analysis are used to explore the sorption mechanism. Se(VI) is sorbed through electrostatic attraction between positive amine groups and negative selenium anions; in a second step, bound Se(VI) is reduced by amine and hydroxyl groups in acidic conditions. A-PEI membranes are successfully used for recovering Se(VI) anions at pH 2. The maximum sorption capacity is close to 83 mg Se g⁻¹; the sorption isotherm is described by the Sips and Langmuir equations. The membranes are poorly sensitive to flow rate in the range 15–50 mL min⁻¹. The kinetic profiles are fitted by the pseudo-first order rate equation. Solute desorption is operated using NaOH solutions; the sorbent shows a remarkable stability in sorption and desorption properties for a minimum of 4 cycles.

Keywords:

Selenium sorption

Alginate-polyethylenimine composite membrane

Isotherms

Kinetics

Recycling

Binding mechanism

1. Introduction

Selenium (Se) is a rare non-metallic chemical element with a double beneficial and harmful character to living organisms: at low concentration, it is an essential nutrient (important role in the proper functioning of the human immune system); while at higher concentration little above homeostatic level, it is a huge threat because of specific toxicity and bio-accumulation [1]. To minimize the possible risks associated with Se, the World Health Organization (WHO) has set a maximum Se concentration in drinking water of 40 µg L⁻¹, while in the European Union (EU) regulations Se concentration should not exceed 10 µg L⁻¹ [2,3]. Therefore, Se removal from surface water, groundwater or wastewater (derived from mining, coal-fired power plants, petrochemical, refineries and agricultural drain) requires a proper treatment in order to

achieve the purification and/or allow the re-use of natural water resources. Another interest for Se removal from water streams consists of the sustainable recovery and re-use of the element to face future Se scarcity [4]. Selenium may occur under five forms in geochemical environments: selenide (Se(-II)), elemental Se (Se(0)), selenite (Se(IV)), selenate (Se(VI)) and organic Se. However, Se(IV) and Se(VI) are the predominant species in aqueous systems [5]. Although both Se(IV) and Se(VI) could bioaccumulate in organisms and be harmful to health, Se(VI) is found to be of higher toxicity; existing as SeO₄²⁻, HSeO₄²⁻, H₂SeO_{4,aq}. In addition, Se(VI) is more difficult to remove because of the formation of more stable species in aqueous solutions, compared with Se(IV) [6]. The concentration and speciation of Se in wastewater are affected by environmental factors such as pH and redox conditions [7]. Several technologies, including chemical reduction, coagulation, membrane separation, ion exchange and sorption have been proposed to remove Se from aqueous solution [8]. However, in the past few decades, there has been not much literature about treating Se(VI)-containing wastewaters; most of them still in an exploratory stage [2]. Therefore, this study focuses on the removal of Se(VI) ions from

* Corresponding author.

E-mail addresses: Yayuan.Mo@mines-ales.fr (Y. Mo), Thierry.Vincent@mines-ales.fr (T. Vincent), Catherine.Faur@umontpellier.fr (C. Faur), Eric.Guibal@mines-ales.fr (E. Guibal).

aqueous solution using a composite sorbent having anion-exchange properties.

In recent years, sorption has been considered one of the most low-cost, simple and eco-friendly process. Sorption systems have been widely adopted for the removal of oxoanions (e.g., Se(VI), Cr(VI) and As(V)) from wastewater [9]. Among various sorbents recently developed, algae-based adsorbents and their derivatives are considered to be promising sorbents due to their low cost, abundance [10] and high affinity for metal ions and dyes [11]. For example, brown seaweed *Ecklonia* biomass and *Sargassum filipendula* residue of alginate extraction have been successfully used to remove Cr(VI) [12,13]. As(III) removal using green algae (*Maugeotia genuflexa*) biomass has been investigated: sorption capacity reached up to 57.5 mg As g⁻¹ [14]. Tuzen and Sari [4] reported the removal of Se(IV) ions from wastewater by *Cladophora hutchinsiae* (green alga); the maximum biosorption capacity was found to be close to 74.9 mg Se g⁻¹ at pH 5. However, it is noteworthy that some organic compounds of raw algae biomass are readily leached during the sorption process; this may cause, in turn, a secondary pollution. Moreover, the solid-liquid separation of biomass is another problem, especially when the sorbent is used as a powder. Therefore, there is still a need for developing alternative conditionings of algal-based materials having enhanced sorption properties and facilitated operating process. Conditioning these materials as porous beads or foams may represent a solution to these drawbacks.

In the case of brown-algae, the most important biopolymer constituting the cell wall is alginate, a biopolymer constituted of guluronic and mannuronic acids (i.e., monomer units bearing carboxylic acid groups). Alginate is a natural anionic linear polysaccharide and a water-soluble polymer with abundant free carboxyl and hydroxyl groups. It is an excellent gel-forming candidate that can be used combined with other materials to obtain multi-functional sorbents like beads and membranes [15,16]. Alginate has been widely investigated for the binding of metal ions [17] and for the elaboration of advanced materials such as batteries [18]. The affinity of carboxylic groups for divalent cations (though tri-valent cations can also bind to the biopolymer) has been also used for polymer ionotropic gelation.

Using raw algal biomass for preparing composite PEI sorbents avoids using refining processes with limited production of waste sub-products [19]. However, preliminary studies showed a loss in the stability of obtained foams. For this reason, alginate was thus preferred to brown algae biomass for preparing stable and highly porous foams.

Frequently, alginate foams and sponges are obtained playing with various conditions of freezing and drying, but also with the type of metal and biopolymer concentration [20]. Conventional processes for production of foams and sponges (involving freeze-drying) are highly energy consuming. In addition, the thin porosity of resulting foams may also cause supplementary energy consuming during sorption processing.

The objective of the present research consists of developing alternative innovative sorbents based on alginate with high efficiency in natural drainage and increased reactivity for metal ions. This target is achieved by preparing membrane without sophisticated drying procedure: foam structuration is operated using the proper reaction of alginate (anionic functional groups) with amine groups of polyethyleneimine (PEI, cationic reactive groups) [21], followed by the stabilizing crosslinking of primary amine groups (on PEI) with glutaraldehyde. The cross-effects of PEI interactions with alginate and PEI crosslinking with glutaraldehyde are expected to contribute to the chemical stability of the composite but also its physical stability during the drying step. This original method is also introducing complementary amine groups, which are highly reactive for metal binding. The high porosity of the membranes is offering outstanding natural drainage properties (low energy consuming at operating). This property combined with high affinity for anions is expected to open new perspectives for simple operating processes in wastewater treatment but also for

supported catalysis, or antimicrobial applications (after binding specific metal ions).

A series of analytical procedures (including titration for measurement of pH_{PZC}, FTIR and XPS spectroscopies) is used for characterizing the material. The new sorbent is carried out for Se(VI) sorption in recirculation mode (the membrane being immobilized in a mini-column). Sorption properties are considered with investigation of pH effect, uptake kinetics, sorption isotherms, effect of co-existing ions and sorbent recycling.

2. Materials and methods

2.1. Materials

Alginate powder was purchased from FMC BioPolymer (Ayr, UK). Previous analyses have characterized the biopolymer [22]:

- weight-average molar mass (Mw) of 4.46×10^5 g mol⁻¹ (determined by the equation $[\eta] = 0.023 \times Mw^{0.984}$ [23], where the intrinsic viscosities $[\eta]$ were measured with an Ubbelohde-type viscometer (falling-ball viscosimeter, AMV-200 Anton Paar GmbH, Graz, Austria) (using 0.1 M NaCl salt as the background salt in the solvent phase) at 25 °C.
- mannuronic to guluronic acid (M/G) ratio of 0.16/0.84 (obtained by ¹³C NMR using a Bruker Avance 400 spectrometer, Billerica, MA, USA).

A homogeneous alginate solution (4%, w/w) was prepared by mixing appropriate amount of alginate powder with demineralized water (under vigorous stirring) at room temperature. Branched polyethyleneimine (PEI, 50% w/w, molecular weight close to 7.5×10^5 g mol⁻¹) and glutaraldehyde (GA, 50%, w/w in water) solutions were supplied by Sigma-Aldrich (Saint-Louis, USA). The working PEI solution (4%, w/w) was obtained by dilution with demineralized water and pH control to 6.5 using HNO₃ solution.

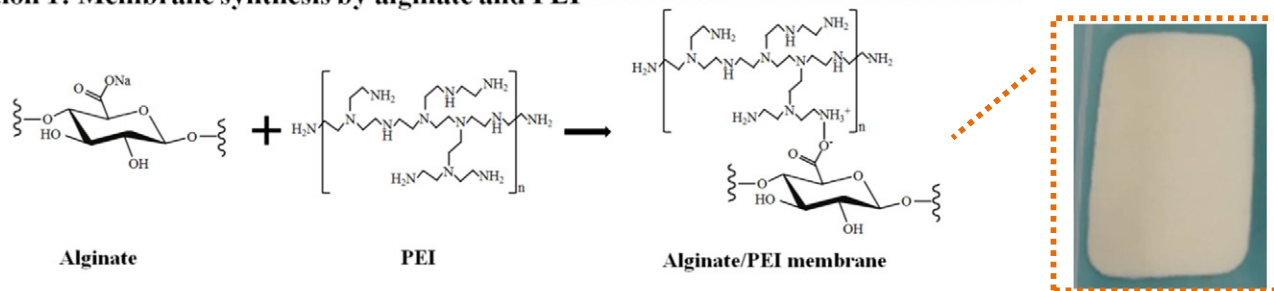
2.2. Synthesis of A-PEI membranes

Scheme 1 shows an illustration of the synthesis of the membrane using alginate, PEI and GA is shown in Scheme 1. Briefly, the membrane was prepared by diluting 100 g of 4% alginate solution with demineralized water to 500 g and stirring until obtaining a homogeneous solution. In a second step, 35 mL of 4% PEI solution (pH controlled to 6.5) was added into the solution under stirring. Next, the mixture was rapidly poured into a rectangular mold and maintained at room temperature for 24 h to complete the reaction between PEI and alginate and to form the membrane (Reaction (1), see Scheme 1). Fabricated membranes can be shaped into different thicknesses using different molds. Afterwards, for strengthening the stability of the composite membrane a crosslinking treatment was applied: 2.5 mL of 50% GA was added into the mold with 300 mL of demineralized water before immersing the membrane (which was previously carefully washed with deionized water, four times) at room temperature (Reaction (2), see Scheme 1). Finally, after 24 h of slow shaking (30 rpm) the membrane was again carefully washed with deionized water and air-dried at room temperature. The membrane was cut into discs (25 mm diameter) for sorption tests.

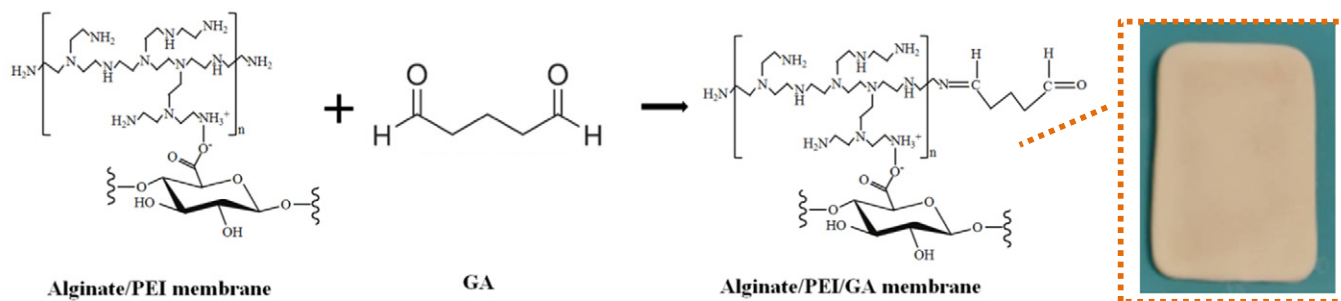
2.3. Characterization of A-PEI membranes

For the analysis of the membrane (before and after Se(VI) sorption, and desorption), FTIR spectra were obtained using an FTIR spectrometer equipped with an ATR (Attenuated Total Reflectance tool, Bruker VERTEX70 spectrometer, Bruker, Billerica, MA, USA) within the 4000–400 cm⁻¹ region to verify the presence of functional groups in the membrane (and their changes after selenium binding and release). The surface morphology and elemental composition of membranes

Reaction 1: Membrane synthesis by alginate and PEI



Reaction 2: Crosslinking by GA



Scheme 1. Synthesis of A-PEI membranes.

before and after Se(VI) sorption were characterized using a scanning electron microscope (SEM, Quanta FEG 200, Thermo Fisher Scientific, Mérégnac, France) equipped with an Energy dispersive X-ray accessory (EDX, Oxford Instruments France, Saclay, France). X-ray photoelectron spectroscopy (XPS) analysis was carried on a ESCALAB 250XI spectrometer (Thermo Fisher Scientific, Waltham, MA, USA) with a monochromatic Al K_{α} radiation ($h\nu = 1486.6$ eV) and a passing energy of 50 eV.

The point of zero charge (pH_{pzc}) of the membrane was determined using batch equilibrium techniques [24]: 0.15 g of membrane was shaken in polyethylene bottles with 40 mL of 0.1 M NaCl solution for 48 h, at different initial pH values (pH_0 , in the range 2–10). Then, the final pH (pH_f) was measured and plotted against pH_0 . The pH_{pzc} corresponds to $\text{pH}_f = \text{pH}_0$.

In addition, other properties of the membrane, such as mechanical stability, density, porosity and water flux were also measured and repeated (at least twice). A certain amount of membrane disc was immersed in 20 mL of demineralized water in polyethylene bottle and shaken (reciprocal shaker frequency: 150 rpm) for 72 h. The membrane disc was weighed after shaking and drying to calculate mechanical stability ($\text{stability} (\%) = 100 m_{\text{eq}}/m_0$, where m_0 (mg) and m_{eq} (mg) are the mass of the membrane before and after shaking). On the other side, the static stability of the membrane was also tested by fixing the membrane in a column device, which was continuously fed for 3 days at pump speed of 15 mL min^{-1} . Water flux (J) was obtained by measuring the time consumed (t) for passing 100 mL (pure water) from the same hydraulic level (h , fixed) through the membrane disc at 20°C and 0.006 bar (calculated from the water height by $p = \rho \times g \times h$). The flux was calculated by the equation: $J = V_p/(A \times t)$. The effective area (A) of the membrane is 4.64 cm^2 . The density and porosity of the membrane was measured according to pycnometer measurement method, using ethanol as the solvent [25]. In brief, it was determined by measuring the total volume of porous membranes and the amount of ethanol required to fill the porous compartment.

2.4. Se(VI) sorption and desorption experiments

All sorption experiments were conducted in a continuous column device (Figure AM1, see Additional Material Section, AMS). A 2 g L^{-1}

Se(VI) stock solution was prepared by dissolving appropriate amount of sodium selenate ($\text{Na}_2\text{SeO}_4 \cdot 10\text{H}_2\text{O}$, BDH Chemicals Ltd., Poole, England) in water; working solutions were prepared by water dilution of stock solution prior to target experiment. The effect of pH was conducted in the initial pH range of 1–7 (adjusted by HCl or NaOH) with a fixed Se(VI) concentration of 100 mg L^{-1} and a sorbent dosage of 0.8 g L^{-1} . After reacting 24 h, at flow rate of 15 mL min^{-1} , the equilibrium pH_{eq} of solution was measured by a pH-meter Cyber Scan pH 6000 (Eutech instruments, Nijkerk, the Netherlands). The samples were subsequently filtered through filter papers ($\varnothing 25 \text{ mm}$, 1–2 μm pore size, Prat-Dumas, France); the residual Se concentration was analyzed by ICP-AES. Sorption isotherm was assessed at varying initial concentrations (10–270 mg Se L^{-1}) with a sorbent dose of 0.8 g L^{-1} at pH 2. After the reaction reaches equilibrium, residual Se concentration in collected sample was determined by ICP-AES. Sorption kinetics of Se(VI) on membrane were investigated using batch tests at three different flow rates (5, 15 and 50 mL min^{-1} ; i.e., superficial flow velocities: 0.65, 1.94 and 6.47 m h^{-1}). The tests were carried out by contact, in a recirculation mode, of 200 mg of the membranes with 500 mL of 50 mg Se L^{-1} solution at pH 2. A 2-mL aliquot was collected at specified time intervals and immediately filtered for Se analysis.

The presence of a large number of protonated amine groups in the membrane in acidic solutions lets suspect a high affinity for anions (including selenate anions). Sorption tests were performed in the presence of increasing concentrations of commonly co-existing anions, such as Cl^- , NO_3^- , and SO_4^{2-} . The concentration of coexisting anions ranged from 0 to 800 mg L^{-1} . These experiments were carried out by contacting 50 mg of the membranes with 50 mL of 100 mg L^{-1} Se(VI) solution (at pH 2) containing co-existing anions. After reacting in recirculation mode at flow rate of 15 mL min^{-1} for 24 h, the supernatant was filtered off for analyzing residual concentration.

Four cycles of sorption–desorption were carried out to evaluate the reusability of the membrane. For each sorption experiment, 40 mg of membrane were contacted with 50 mL of 100 mg Se L^{-1} Se (VI) at pH 2, and then the solution was collected and filtered after reaching sorption equilibrium. For the desorption experiment, the Se-loaded membrane was contacted with 50 mL 0.01 M NaOH

solution for 30 min; selenium concentration was determined on residual filtrated solution. After washing and drying, the regenerated membrane was re-used in the next cycle.

In addition, to evaluate the repeatability of the membrane sorption performance (and membrane synthesis), two identical membranes were fabricated at different times and used to adsorb Se(VI). The results are shown in Figure AM2 (see AMS).

2.5. Analytical methods

Selected experiments were conducted in parallel and the data were presented as the values of average and standard deviation (SD). After experiments, the initial and residual concentrations of total Se in the supernatants were determined using an inductively coupled plasma atomic emission spectrometry (ICP-AES, JY Activa M, Jobin-Yvon, Horiba, Longjumeau, France). The sorption capacity (q_{eq} , mg Se g^{-1}) of membrane was calculated by the mass-balance equation: $q_{eq} = (C_0 - C_{eq}) \times V/m$, where C_0 and C_{eq} are the initial and residual concentrations (mg Se L^{-1}), respectively, V is the volume of solution (L) and m the dry weight of membrane sorbent (g). The desorption efficiency (DE, %) of membrane was calculated using the equation: DE (%) = (amount of Se desorbed / amount of Se sorbed) \times 100.

3. Results and discussion

3.1. Properties of membrane

The tests of membranes for mechanical stability show that the material loses less than 14% under vigorous agitation (i.e., 150 rpm). This means that the material has a high mechanical stability and can maintain its integrity under a high-speed shaking in water. Considering that the preferred mode of application is fixing the membranes in a column device, the static stability of the membrane (measured under constant feeding for 3 days) in the column device is also measured (material loss does not exceed 3%). This confirms that the material is highly stable in fixed-bed column.

In addition, the SEM test is used for observing the physical structures and morphologies of the material. The surface and cross-section morphologies of the membrane are shown in Fig. 1. The material has a porous structure with considerable macro-porosity. This means that the membrane is widely opened, which keeps high-permeability for water transfer. Pycnometer measurements show that the density and porosity of the membrane are 0.048 $g\ cm^{-3}$ and 74%, respectively. The water flux of the membrane is 13 $mL\ cm^{-2}\ min^{-1}$ at 0.006 bar, which means

superficial flow velocities as high as 7.8 $m\ h^{-1}$ can be reached (under constant feed to maintain water column depth, with draining conditions). This clearly demonstrates the highly percolating properties of the membranes compared to most of reported similar membranes (Table AM1, see AMS). Despite lower pressure applied to the membrane (corresponding to natural drainage conditions), the water flux of A-PEI membrane is over-performing compared with reference materials.

EDX analysis gives the semi-quantitative elemental composition of the membrane (Figure AM3, see AMS). The spectrum of raw membrane (see Figure AM3c) shows that the material mainly consists of C and O elements (exceed 95% in total, tracers of the organic fraction) but also Ca, Na, Cl, K, S, Mg and Al elements (as residues of the extraction and shaping process of alginate). Figure AM3d confirms selenium binding with the appearance of selenium peaks.

The FT-IR analysis allows identifying the chemical groups present on the membrane (Figure AM4, see AMS). For raw membrane, the main bands are identified: the strong and wide band at 3200–3500 cm^{-1} is assigned to the overlapping of O—H and N—H stretching vibrations [26]; the weak band around 2927 cm^{-1} is attributed to the stretching vibration of C—H [27]. Strong absorption band at 1596 cm^{-1} and medium absorption band at 1317 cm^{-1} are characteristic peaks of overlapping of C=N and N—H vibration and C—N stretching vibration, respectively. This is attributed to the reaction between amine groups of PEI and aldehyde groups of GA [19,28]. Schiff bases are formed during the crosslinking of PEI with GA; amide groups appear on the membrane, which contribute to substantially improving its sorption capacity, especially for anions (e.g., Se(VI)). The band at 1404 cm^{-1} is assigned to the symmetric stretching of COO⁻ group of the alginate [29]. Meanwhile, the bands at 1087 and 1029 cm^{-1} are associated with C—O stretching vibration [30] and 947 and 885 cm^{-1} are C—H bending vibrations [31]. These findings mean that hydroxyl, carboxyl, amino groups in the membrane might play important roles in the binding of selenium ions.

It is noteworthy that the conjugate acid dissociation constant (pK_a) of carboxylic groups in alginate are 3.38 for mannuronic and 3.65 for guluronic acid [32], while the pK_a values of amine groups in PEI are usually reported at 4.5, 6.7 and 11.6 for primary, secondary and tertiary amines, respectively [33]. In addition, the pH_{pZC} of membrane determined in the pH range of 1.0 to 10.0 was found to be 6.3; this means the reactive groups are mostly protonated below pH 6 (overall positive charge). The charges on the surface of membrane are positive; this opens the way to the sorption of negatively charged selenium anions by electrostatic attraction (Coulombic of negatively charge selenate species by protonated amine groups, preferentially primary amine groups).

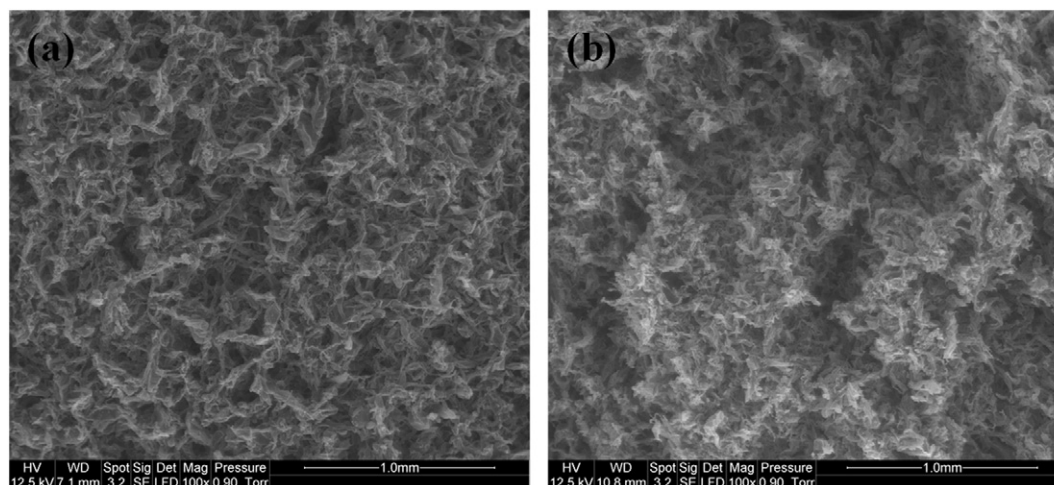


Fig. 1. Porous structure of membranes (SEM micrographs) (a) Surface and (b) Cross-section (bar: 1 mm).

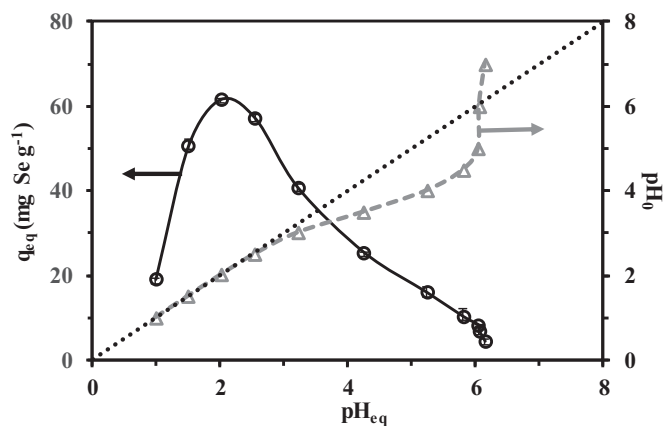


Fig. 2. Effect of pH on Se(VI) sorption using membrane (C_0 : 100 mg Se L⁻¹; Sorbent dosage: 0.8 g L⁻¹; contact time: 24 h; flow rate: 15 mL min⁻¹; temperature, T: 20 ± 1 °C; dashed line represents pH variation during sorption).

3.2. Sorption study

3.2.1. Effect of pH on Se(VI) sorption by membranes

The pH is a critical parameter in the evaluation (and understanding) of sorption properties of a sorbent for metal ions (and more generally charged species). Indeed, this parameter has a dual effect on the speciation of metal ions (including metalloid ions) in solution (depending also on the presence of ligands) and on the charge characteristics of sorbent surface. Fig. 2 shows the effect of pH variation between 1 and 7. Under selected experimental conditions, maximum Se(VI) sorption capacity reaches 61.7 mg g⁻¹ at pH 2. Similar sharp optimum (between pH 2.5 and 3.5) was reported for the recovery of both Se(IV) and Se(VI) using eggshell membrane and chicken feather [34]. The pH_{PZC} of 6.3 for membrane means that in acidic solution (pH below 6), the overall charge on membrane surface is positive: selenate anions may be electrostatically attracted on protonated amine groups. At pH below 1.5, the competitor anions Cl⁻ (due to acid dissociation) strongly limits the sorption capacity. In addition, selenate anions is mainly present as hydrogenoselenate. Peng et al. [35] reported, for the different transitions of H₂SeO₄/HSeO₄⁻/SeO₄²⁻, the strong acid character of selenic acid (i.e., non-significant pK_{a1}) and pK_{a2} value close to 1.9. Figure AM5a (see AMS) shows the distribution of main selenate species in function of pH. Below pH 1.5, selenate ions are mainly protonated (as selenic acid or hydrogenoselenate, HSeO₄⁻): this may weaken the electrostatic attraction between the reactive groups and selenate species.

When the pH increases from 2 to 7, the sorption capacity decreases to 8.3 mg g⁻¹. The protonation of amine groups progressively decreases and the speciation of selenate is displaced to different predominating species. Figure AM5a (see AMS) shows the speciation of primary and secondary amine groups; tertiary amine groups remain protonated in the studied pH range.

The comparison of the distribution of SeO₄²⁻ and HSeO₄⁻ species with the sorption efficiency suggests that selenium binding drastically increases when divalent anionic species predominates over monovalent species (in the range pH 1–2). In this pH range, primary amine groups are fully protonated.

Above pH 2, despite the predominance of divalent selenate species (most favorable species for binding to protonated amine groups), the sorption capacity strongly decreases. This can be associated to the progressive decrease of the protonation of primary amine groups. The pK_a of primary amine groups is close to 4.5 in high molecular PEI [33]. The partial cross-linking of amine groups with aldehyde groups (of the cross-linker agent) may affect the acid-base properties of these amines but the reactive groups remain basic enough for maintaining convenient protonation/deprotonation pattern.

In the pH range 3.5–5.5, the sorption capacity decreases more weakly: primary amine groups are progressively deprotonated but secondary amine groups (with less affinity for selenate anions) may contribute to weak sorption. At pH above 5.5, the secondary amine groups begin to deprotonate and a new stronger decrease in sorption capacity is observed.

These observations tend to demonstrate that the probable mechanism involved in Se(VI) binding consists of the electrostatic attraction of preferentially SeO₄²⁻ (divalent anion) onto protonated primary amine groups (preferentially to secondary amine groups). This means also that an appropriate crosslinking ratio (between primary amine groups and aldehyde groups) should take into account the necessary stabilization of the sorbent but also the availability of primary amine groups. In the case of the sorption of anionic Se species on non-living *Eichornis crassipes* and *Lemna minor*, the possible contribution of Coulombic interaction with protonated hydroxyl groups (in acidic solutions) has been also reported [36].

Fig. 2 also shows the pH change during the sorption process. Between pH 2 and 3.5, the pH remains stable, despite the sorption of Se(VI); proton capture and selenate binding are low enough compared to the actual amount of protons to maintain unchanged the pH. In the pH range 3.5–5.5, the equilibrium pH tends to substantially increase (by up to 1 pH unit). These trends are confirmed in Figure AM5b (see AMS). pH variations during sorption are compared to pH variations from background salt solutions (results collected from titration data in the determination of pH_{PZC}). The pH variation is negligible in the optimum pH range of sorption but substantially increases at pH higher than 3–4. At higher initial pH (i.e., 7), the equilibrium pH tends to decrease, while at pH 6.1 the pH tends to stabilize. This can be directly correlated to the pH_{PZC} value (i.e., 6.3). The pH variation is less marked in the case of Se sorption solution (compared with background salt solution). These trends confirm that pH variation is not only due to the proper acid-base properties of the sorbent but that the interaction with selenate species contributes to moderate the pH variation.

Figure AM6 (see AMS) shows the plot of the distribution ratio ($\log_{10}D = q_{eq}/C_{eq}$, L g⁻¹) vs. equilibrium pH (log–log plot). The slope of linear sections is frequently associated with the stoichiometry of the ion-exchange between sorbed species and counter-ion(s) released from the sorbent. The optimum pH is confirmed close to pH 2. Two segments roughly linear can be identified corresponding to the increase of sorption with pH (from 1 to 2) with a slope close to 0.7 (the points at pH 1 are shifting the slope to higher value compared to the points between pH 1.5 and 2; slope close to 0.3). The average value close to 0.5 could be associated with the binding of SeO₄²⁻ (consistently with the predominating species in this pH range); this means that two protonated amine groups are involved in the binding of one selenate ion (selenate/amine molar ratio close to 0.5). At pH higher than 2, the sorption capacity decreases and the slope of the curve is close to 0.27, as an evidence of (a) the change in the interaction mode between amine groups and selenium species and (b) the effect of acid-base characteristics of the sorbent. Further experiments were performed at pH 2.

3.2.2. Effect of flow rate on uptake kinetics

The uptake kinetics can be controlled by the diffusion mass transfer process and the proper sorption reaction at the liquid/solid interface [37]. In fixed-bed columns, the flow rates may have potential impact on mass transfer (through resistance to film diffusion, to intraparticle diffusion) but also on eventual preferential channeling. In the case of materials with non-homogeneous distribution and size of channels, the solution may pass through the largest pores. This may occur at the expense of longer transfer zone and earlier breakthrough (or longer equilibrium time), and even a non-saturation of certain parts of the foam. Imposing a higher flow rate may help accessing the complete reactive volume and surface of the membrane. This may be explained by the fact that a lower flow rate (5 mL min⁻¹) slows down the flux inside the membrane (this limits the hydrodynamic transfer of the solution in

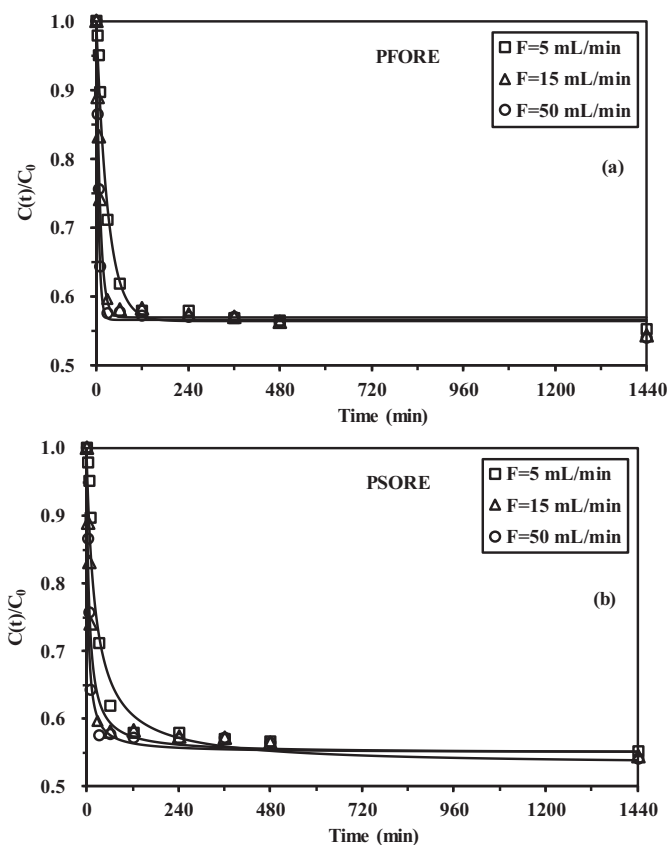


Fig. 3. Se(VI) uptake kinetics – Effect of flow rate (C_0 : 50 mg Se L⁻¹; SD: 0.4 g L⁻¹; pH₀: 2; T: 20 ± 1 °C; solid line: fit of kinetic profile with the PFORE (a) and the PSORE(b)).

the whole mass of the membrane), and increases the resistance of air bubbles (which may limit the contact of the solution with reactive groups) [38]. In order to verify this effect and to determine the minimum flow rate (or superficial flow velocity) experiments are compared at different flow rates (i.e., 5, 15 and 50 mL min⁻¹). In the case of membranes immobilized in column under recirculation mode, the system is globally analogous to a continuously stirred reactor and the flow velocity is analogous to the agitation speed parameter (complicated by the possible occurrence of channel effects). Fig. 3 compares the kinetic profiles for the sorption of Se(VI); the contact time for equilibrium was set to 24 h. The flow rate hardly affects residual concentration; under selected experimental conditions, the recovery yield reaches 46% (sorption capacity close to 60 mg Se g⁻¹). The equilibrium time is almost unchanged when varying the flow rate between 15 and 50 mL min⁻¹, 30 min are sufficient while at the lowest flow rate (i.e., 5 mL min⁻¹) the equilibrium time increases up to 120 min. The limit flow rate for avoiding channeling effects is close to 15 mL min⁻¹ (i.e; superficial flow velocity: 1.93 m h⁻¹).

The proper reaction rate may be approached using the pseudo-first order rate equation (PFORE) or the pseudo-second order rate equation (PSORE), which are commonly used to model chemical reactions [39].

These equations (Eqs. (1) and (2)), initially designed for modelling homogeneous chemical reactions, have been successfully used for describing heterogeneous systems. However, in these cases, the rate coefficients are considered apparent rate constants that integrate the contribution of diffusion mechanisms.

$$\text{PFORE} : q(t) = q_{eq,1}(1 - e^{k_1 t}) \quad (1)$$

$$\text{PSORE} : q(t) = \frac{q_{eq,2}^2 \times k_2 \times t}{1 + q_{eq,2} \times k_2 \times t} \quad (2)$$

where $q_{eq,i}$ (mg g⁻¹) and $q(t)$ (mg g⁻¹) are the amount of Se(VI) sorbed onto membranes at equilibrium and at time t ($i = 1$ or 2), respectively, and k_1 (min⁻¹) and k_2 (g mg⁻¹ min⁻¹) are the rate constants of PFORE and PSORE models, respectively. PSORE is usually associated to systems controlled by chemisorption, contrary to PFORE associated with physical-sorption [40].

The parameters of the PFORE and PSORE for Se(VI) sorption kinetics using three different flow rates are listed in Table 1; they were determined by non-linear regression using Mathematica® software. In Fig. 3, the solid lines represent the simulated curves for PFORE and PSORE using the calculated parameters summarized in Table 1. The comparison of the determination coefficients (R^2) shows that the PFORE equation fits better kinetic profiles. This is confirmed by the superimposition of fitted curves with experimental points. However, it is noteworthy that the calculated values for the equilibrium sorption capacity (i.e., $q_{eq,i}$) PSORE profiles are more accurate than PFORE simulated curves. Here, the preferential fit of experimental data with the PFORE can be explained by the electrostatic attraction mechanism between anionic selenate species and protonated amine groups (i.e., physisorption). The apparent rate coefficients strongly increase with the flow rate: between 5 and 15 mL min⁻¹, the k_1 coefficient varies proportionally (i.e., from 3.30×10^{-2} to 9.93×10^{-2} min⁻¹) while above, at 50 mL min⁻¹, the coefficient progression tends to level off (at 17.2×10^{-2} min⁻¹). Similar trends are observed for the evolution of the apparent rate coefficient for PSORE modeling (i.e., k_2 in Table 1).

3.2.3. Sorption isotherms

The sorption isotherm, which plots the sorption capacity in function of residual concentration at fixed temperature and pH, provides important information on the affinity of the sorbent for the solute. Fig. 4 shows Se(VI) sorption isotherm at pH 2. The sorption capacity steeply increases at low concentration (below 25 mg Se L⁻¹) before progressing more weakly. A pseudo-saturation plateau is reached around 83 mg Se g⁻¹ (for residual concentrations higher than 150 mg Se L⁻¹). The sorption isotherms can be modeled using various equations [41]; however, the most frequently used are the mechanistic Langmuir equation (Eq. (3)) and empirical models such as the Freundlich (Eq. (4)) and the Sips (Eq. (5)) equations. The Langmuir model assumes that the sorption proceeds as a monolayer at the homogeneous surface of the sorbent [42], while the Freundlich model is assigned to non-ideal sorption on heterogeneous surfaces as well as multilayer sorption [43]. The Sips equation (also called Langmuir-Freundlich equation) is a

Table 1
Effect of flow rate on Se(VI) uptake kinetics – Comparison of fitting equations.

Models	Parameters	F = 5 mL min ⁻¹	F = 15 mL min ⁻¹	F = 50 mL min ⁻¹
PFORE	$q_{eq,exp}$ (mg g ⁻¹)	60.9	60.1	60.9
	$q_{eq,cal}$ (mg g ⁻¹)	59.0	56.7	57.4
	$k_1 \times 10^2$ (min ⁻¹)	3.30	9.93	17.2
	R^2	0.997	0.992	0.996
PSORE	$q_{eq,cal}$ (mg g ⁻¹)	63.8	59.4	59.5
	$k_2 \times 10^3$ (g mg ⁻¹ min ⁻¹)	0.69	2.46	4.49
	R^2	0.984	0.990	0.988

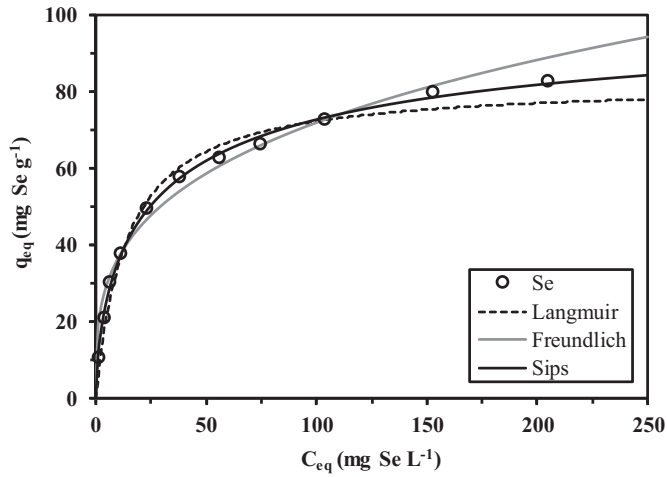


Fig. 4. Se(VI) sorption isotherms using membranes (SD: 0.8 g L⁻¹; contact time: 24 h; pH: 2; flow rate: 15 mL min⁻¹; T: 20 ± 1 °C).

combination of the two models, based on pure mathematical concept.

$$\text{Langmuir} : q_{eq} = \frac{q_{m,L} \times b_L \times C_{eq}}{1 + b_L \times C_{eq}} \quad (3)$$

$$\text{Freundlich} : q_{eq} = k_F C_{eq}^{1/n_F} \quad (4)$$

$$\text{Sips} : q_{eq} = \frac{q_{m,S} \times b_S \times C_{eq}^{1/n_S}}{1 + b_S \times C_{eq}^{1/n_S}} \quad (5)$$

where C_{eq} (mg Se L⁻¹) is the equilibrium concentration of Se(VI); q_{eq} , $q_{m,L}$ and $q_{m,S}$ (mg Se g⁻¹) are the equilibrium concentration and the maximum sorption capacities calculated from Langmuir and Sips equations, respectively. The coefficients b_L and b_S (L mg⁻¹) are the Langmuir constants for Langmuir and Sips equations, respectively; k_F is the Freundlich constant, and n_F and n_S represent sorption intensity parameters for Freundlich and Sips equations, respectively.

The lines in Fig. 4 show the fits of experimental data with the three models and the parameters reported in Table 2 (parameters determined by non-linear regression analysis). The three models fit well the data in the pseudo linear section (Henry domain) of the sorption isotherm. The Langmuir equation respects the shape of the curve up to a residual concentration close to 103 mg Se L⁻¹ and then diverges and underestimates the sorption capacity in the saturation domain. The maximum sorption capacity at saturation of the monolayer is consistent with the effective maximum sorption capacity (i.e., 82.3 mg Se g⁻¹ vs. 83 mg Se g⁻¹). The Freundlich equation underestimates sorption capacity in the intermediary domain (highest curvature) and overestimates the q_{eq} in the saturation domain; this is a power-type function non-consistent with

Table 2
Se(VI) sorption isotherms – Modeling.

Model	Parameter	
Langmuir	$q_{m,L,cal}$ (mg g ⁻¹)	82.4
	b_L (L mg ⁻¹)	0.072
	R_L	0.04–0.59
	R^2	0.978
Freundlich	k_F (mg g ⁻¹)/(L mg ⁻¹) ^{1/n}	18.46
	n_F	3.385
	R^2	0.965
	Sips	$q_{m,S,cal}$ (mg g ⁻¹)
	b_S (L mg ⁻¹)	0.115
	n_S	1.548
	R^2	0.997

Table 3
Se(VI) sorption capacities of a series of sorbents reported in literature.

Sorbents	pH	C_0^a (mg L ⁻¹)	q_m (mg g ⁻¹)	Ref.
Fe–Mn hydrous oxides	4	5–500	19.8	[72]
Thiourea-formaldehyde resin	5 M	100–500	526	[46]
Purolite S108 resin	HCl			
	3.56	0–856	3.23	[73]
Oxidized multi-walled carbon nanotubes	7	0.5–2	1.87	[74]
Al(III)/SiO ₂ binary oxide system	5	0–237	11.3	[75]
Chloride hydrocalumite Friedel phase	8	36–1086	196	[47]
Al ₂ O ₃ impregnated chitosan beads	6	0–3.8 ^b	20.1	[53]
Chitosan	6	0–15 ^b	2.01	[76]
MgO nanosheets	10.5	1–100	10.3	[76]
LDH/chitosan nanocomposite	6	0–16 ^b	4.5	[77]
Silica magnetite nanoparticles	n.r.	0–200	46.1	[78]
Functionalized silica magnetite NPs	n.r.	0–200	27.6	[78]
<i>Cladophora hutchinsiae</i>	5	10–400	74.9	[4]
Chitosan/clay composite	4	0–10 ^b	8	[79]
Polyamine-type weakly basic IX resin	6	30–240	134.2	[48]
Eggshell membrane	–	–	37.0	[34]
Chicken feather	–	–	20.7	[34]
A-PEI Membranes	2	10–270	83.0	This study

^a Initial concentration range.

^b Equilibrium concentrations (estimated from the graphs); n.r.: not reported.

the progressive saturation of the sorbent. Best fit is obtained with the Sips equation; using a third parameter logically improves the quality of mathematical fit. However, the maximum sorption capacity is substantially overestimated (close to 105 mg Se g⁻¹). The qualitative evaluation of modeled profiles is consistent with the comparison of determination coefficients in Table 2.

The basic characteristics of the sorption process (obeying the Langmuir equation) can be described by the dimensionless equilibrium parameter, R_L , which is calculated using equation (6) [44].

$$R_L = \frac{1}{1 + b_L \times C_0} \quad (6)$$

where C_0 is the initial concentration (mg Se L⁻¹).

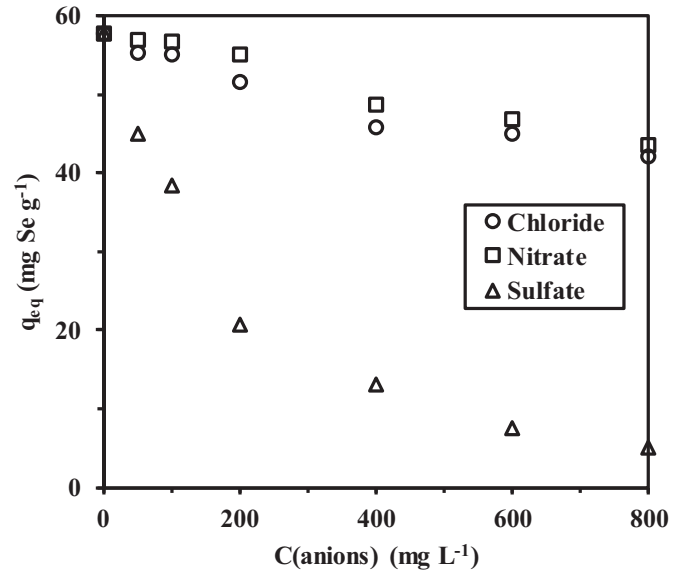


Fig. 5. Effect of coexisting anions on Se(VI) sorption by membranes (C_0 : 100 mg L⁻¹; SD: 1 g L⁻¹; contact time: 24 h; pH: 2; flow rate: 15 mL min⁻¹; temperature: 20 ± 1 °C).

The values of R_L allow qualifying the sorption as unfavorable ($R_L > 1$), linear ($R_L = 1$), favorable ($0 < R_L < 1$) or irreversible ($R_L = 0$) processes [45]. Under selected experimental conditions, the values of R_L vary in the range 0.04–0.59; this confirms that Se(VI) sorption on A-PEI membranes is a favorable process.

Table 3 compares a series of sorption performances (q_m , Langmuir maximum sorption capacity) reported in the literature. Some sorbents such as thiourea-formaldehyde resin [46], chloride hydrocalumite Friedel phase [47] polyamine synthetic resin [48] have remarkable maximum sorption capacities (i.e., 526, 196 mg and 134 Se g⁻¹, respectively); however, in most cases, A-PEI membranes have comparable or higher sorption capacities than alternative sorbents.

3.2.4. Effect of coexisting anions

Coexisting anions such as sulfate, nitrate and chloride are frequently present in natural water streams or industrial effluents. Therefore, considering their potential impact on selenium removal is critical for evaluating the effectiveness of A-PEI membranes for Se(VI) recovery. The sorption capacity of A-PEI membranes for Se(VI) was tested in the presence of increasing concentrations of these competitor anions (50–800 mg L⁻¹). Fig. 5 shows that the three anions inhibited Se(VI) sorption to different extents. Indeed, A-PEI membranes being positively charged in acid solutions have obvious affinity for anions. Monovalent anions, such as chloride and nitrate, have comparable and limited effect on Se(VI) sorption. Under selected experimental conditions, sorption capacity decreases from 57.7 mg Se g⁻¹ to 42.1–43.6 mg Se g⁻¹ (loss in sorption capacity close to 25%) when Cl⁻ or NO₃⁻ concentration reaches up to 800 mg L⁻¹ (i.e., 22.5 mM for Cl⁻ and 12.9 mM for NO₃⁻), which are 17.3 and 9.9 times excess compared to selenium molar concentration (1.3 mM), respectively. In the case of divalent sulfate anions, Se(VI) sorption is almost completely inhibited at sulfate concentration close to 800 mg L⁻¹ (i.e., 8.3 mM, 6.4 times excess): the sorption capacity decreases to 5 mg Se g⁻¹ (i.e., loss exceeds 91%). Figure AM7 (see AMS) shows the impact of competitor anions on Se(VI) distribution ratio (log–log plot). Chloride and nitrate anions have similar behavior with a slope of the plot close to -0.16/-0.17 while for sulfate the slope was close to -1 (i.e., -0.96). These differences clearly illustrate the different competitor mechanism between these anions. Similar phenomenon were reported for the sorption of Se(VI) by iron-oxide-coated sand [49]. The divalent charge of sulfate anions (analogous to the expected bound selenate species, SeO₄²⁻) may explain the strong competitor effect on selenate uptake (direct competitor effect or ion-exchange between sulfate and selenate anions) [50,51]. The chemical analogy between SO₄²⁻ and SeO₄²⁻ was also reported for explaining the strong impact of sulfate competitor anion on Se(VI) recovery using a polyamine weakly basic ionic exchange resin [48]. In the case of hematite modified magnetic nanoparticles [52], the sorption of selenate anions was inhibited by anions (in the range of concentrations: 0–10 mM) according the series: chloride ≈ nitrate (negligible) < sulfate < carbonate << silicate <<< phosphate. The presence of small amounts of sulfate (i.e., 10 ppm) was sufficient for strongly limiting the sorption of both selenite and selenate on nanocrystalline-impregnated chitosan beads [53].

3.2.5. Desorption and recyclability study

Membrane recyclability is a vital parameter for assessing the cost-effectiveness of wastewater treatment. The competitor effect of phosphate was used for promoting the acidic desorption of Se(VI) from Se-loaded marine biomass [36] or the regeneration of Al/Si-Fe/Si coprecipitates [54]. Hydrochloric acid (1 M) solution was used for removing Se(VI) from polyamine-type weakly basic ion exchange resin [48]. In the case of functionalized cellulose, selenate was quantitatively recovered from loaded sorbent using 3 M HCl/2% KClO₃ solutions [55]. Ma et al. [52] used 0.01 M NaOH solutions for Se desorption from hematite modified magnetic nanoparticles.

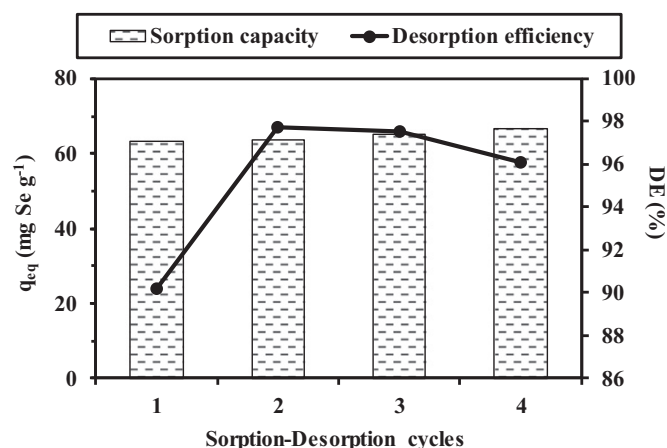


Fig. 6. Se(VI) desorption and sorbent recycling - Se(VI) sorption capacity and desorption efficiency (Sorption step - C₀: 100 mg Se L⁻¹; SD: 0.8 g L⁻¹; pH: 2; flow rate: 15 mL min⁻¹; temperature: 20 ± 1 °C. Desorption step - desorption agent: 0.01 M NaOH; V: 50 mL; time: 30 min; flow rate: 15 mL min⁻¹; temperature: 20 ± 1 °C).

In this study, four consecutive sorption-desorption cycles are carried out using 0.01 M NaOH solution as the eluent to desorb Se(VI). As shown in Fig. 6, the sorption capacity increases slightly from 63 mg g⁻¹ from the first cycle to fourth cycle (under selected experimental conditions). The desorption efficiency is enhanced after the first cycle and then remains over 96% in the subsequent cycles. These results clearly indicate that the membrane has an excellent reusability and that NaOH regeneration allows stable sorption and desorption performances for Se(VI) removal, for at least four cycles. It is noteworthy that the same sorbent was used for chromate recovery from acidic solutions [22]; in this case, chromate desorption was much less efficient (not exceeding 40–50%). Therefore, the recycling of the sorbent was rather limited: the sorption capacity after three cycles was reduced by 60%. These differences between selenate and chromate anions may be explained by the stronger ability of chromate to be reduced in acidic solutions in the presence of organic compounds. The partial degradation (by oxidation) of the sorbent and the *in situ* reduction of Cr(VI) (to form Cr(III)) may explain this progressive depreciation of sorption efficiency. Though selenate can be reduced to selenite, this phenomenon is probably less active compared with chromate/chromium redox reaction (redox potentials: +1.33 V for Cr(VI)/Cr(III) against +1.06 V for Se(VI)/Se(IV) and +0.903 V for Se(VI)/Se(0)).

3.3. Discussion of sorption mechanism

The analysis of pH effect, the selenium speciation and the measurement of p_{H_{pzc}} value suggest that selenate anionic species are immobilized at the surface of the sorbent (on protonated amine groups, preferentially primary amine groups) through electrostatic attraction mechanism. The stoichiometric ratio (i.e., close to 0.5) means that, at the optimum pH, selenate (i.e., SeO₄²⁻) requires two protonated amine groups. In addition, the strong interference of sulfate on selenate sorption confirms that the main bound Se species is probably SeO₄²⁻.

EDX spectra (Figure AM3, see AMS) show selenium ions are found uniformly distributed on the surface of material after Se(VI) treatment; this provides direct evidence for homogeneous selenium sorption onto A-PEI membrane. The significant increase in the intensity of O element after Se(VI) sorption, is directly associated to the binding of the oxoanion [56,57]. Analytical tools may contribute to confirm the interaction mode.

FTIR spectra and the changes in the main bands (before and after Se(VI) sorption, and after Se desorption) are recorded in Figure AM4 and Table AM2 (see AMS). After Se(VI) sorption, the band at 3283 cm⁻¹ (assigned to O—H and N—H stretching vibration) shifts to 3276 cm⁻¹. Simultaneously, a new band at 1712 cm⁻¹ (attributed to

C=O stretching vibration) is observed after Se(VI) sorption; this may be explained by the partial oxidation of some reactive groups [58]. The intensities of the bands at 1596 cm⁻¹ and 1404 cm⁻¹ decrease; these bands are assigned to C=N and N—H vibration in PEI-GA and COO⁻ symmetric stretching in alginate, respectively. The band at 1317 cm⁻¹ (attributed to C—N stretching vibration) shifts to 1294 cm⁻¹. These changes reveal that hydroxyl and carboxyl groups on alginate and amino groups from PEI-GA are involved in Se(VI) binding (mainly amine groups). In addition, subsequent reduction may occur; possibly on carbonyl/carboxyl groups of alginate. The appearance of a strong band at 864 cm⁻¹, which can mask the band of 885 cm⁻¹ after sorption, could be attributed to the presence of Se—O bond, as reported by Peak and Sparks [59] and Chubar [60], which illustrated the formation of complexes between selenate and relevant sorbents. Moreover, changes of bands at 810 cm⁻¹ and 773 cm⁻¹ may also be caused by selenate sorption followed by *in situ* reduction [61,62]. Indeed, Elder et al. [63] also reported that the IR spectra of free SeO₃²⁻ in solution exhibits a peak at 810 cm⁻¹ (symmetric stretching vibration), while the intensity of the peak at 740 cm⁻¹ decreases (asymmetric stretching vibration). After selenium desorption, the spectrum of the material shows only minor changes compared with the spectrum of raw A-PEI membrane. The broad band (overlapping of O—H and N—H stretching vibrations) is shifted to 3220 cm⁻¹ after desorption by NaOH solution. It is noteworthy that the bands between 900 and 750 cm⁻¹ (on the spectrum of Se-loaded A-PEI membrane) are shifted back to their original positions on the spectrum of raw A-PEI membrane; this confirms that selenium is almost completely desorbed, and that the material is perfectly regenerated.

The XPS analyses of raw, Se-loaded and Se-desorbed membranes are carried out to obtain more detailed information on sorption mechanisms through the determination of functional groups and Se oxidation state. Figure AM8 (see AMS) shows XPS survey spectra of the membranes. Small peaks appear around binding energies (BEs) of 58.7 eV and 164.7 eV for Se 3d and Se 3p on Se(VI)-loaded membrane, indicating the accumulation of Se on the sorbents. Table 4 and Fig. 7 reports the identification of the most representative elements (i.e., C, N, O and Se) observed on the XPS survey spectra for raw, Se(VI) loaded and Se-desorbed membranes. Due to the partial overlapping of the S 2p and the Se 3p, it appears preferable discussing Se 3d band. The spectrum of Se 3d was deconvoluted with three peaks at binding energies of 54.6, 55.7 and 58.7 eV, which can be assigned to the oxidation state of Se(-II), Se(0) and Se(IV), with peak areas (atomic fractions) of 10.1, 5.5 and 84.4%, respectively [64,65]. This means Se(VI) (initially present in the solution, and supposed to appear at BE: 61 eV) is not observed in

the Se 3d spectrum after being immobilized on the sorbent (see Table 4): Se(VI) ions are mostly reduced to Se(IV) on A-PEI membranes.

The C 1s spectra of raw membrane can be deconvoluted into four individual component peaks with BEs of 284.0, 284.6, 285.4 and 287.1 eV, which are assigned to C—C, C—C/C=C/C—H [66], C—N and C=N/C—O groups [67], respectively. These assignments reflect the functional groups in the alginate/PEI/GA membrane. It is noteworthy that the peak area (atomic content) of C=N/C—O decreased from 8.02% to 6.07% after sorption, meaning that the amide or hydroxyl groups participate in the sorption of Se(VI) (or, at least, that their immediate environment is affected by Se binding). Furthermore, the deconvolution of the O 1s spectra of the samples shows two peaks with BEs of 529.8 and 531.5 eV (for raw membrane). These peaks can be assigned to O element in C=O and C—O, respectively [68]. After Se(VI) sorption, the peak area of C=O increases from 8.2% to 9.4% while the peak area of C—O decreases from 91.8% to 90.6%. These weak changes could be explained by partial degradation associated with the reduction of Se(VI) at pH 2; these groups react as electron donors, according Eq. (7) [69]. These observations are consistent with the changes on FTIR spectra (Figure AM4, see AMS).

Fig. 7 also shows the N 1s XPS spectra and the shifts and change in intensity of the different forms of N reactive groups (before and after Se sorption). The N 1s spectrum of A-PEI membrane is decomposed into three individual components at BEs of 398.4, 399.7 and 400.8 eV, which can be assigned to N into —N= (imine group that was generated during the reaction of PEI and GA, see Scheme 1), —NH₂ and —NH₃⁺ compounds, respectively [70]. After Se(VI) binding, the peak with BE at 399.7 eV (i.e., —NH₂) disappears; amine group on PEI contributes to Se(VI) sorption. The content of —N= groups increases (from 64.6 to 68.4%), this can be explained by the partial oxidation of some amino groups by Se(VI) species at pH = 2, as described by Eq. (8). Qiu et al. [71] found similar results in the study of Cr(VI) removal by PEI-modified ethyl cellulose: both the amine groups of PEI and the hydroxyl groups of ethyl cellulose participated in the Cr(VI) reduction reaction. This series of chemical reactions occurring during Se(VI) sorption on A-PEI membrane are also consistent with kinetic profiles: (a) first fast step of sorption, followed by (b) slower mass transfer into the thin scaffold foils of the material together with the proper reduction phenomenon.

After selenium desorption by NaOH solution, the atomic fraction of —NH₃⁺ decreases from 32% to 1.3% (due to deprotonation); deprotonation contributes to decreasing the affinity of the sorbent for selenium anionic species (based on XPS analysis, mainly selenite) and to improve selenium desorption.



The plausible mechanism of Se(VI) sorption onto A-PEI membrane consists of:

- first binding of Se(VI) anions by electrostatic attraction on protonated amine groups of the sorbent (preferentially primary amines), followed by
- the *in situ* reduction of Se(VI) to Se(-II), Se(0) and Se(IV) (with the help of H⁺ and electron-donor groups including amines, aldehyde, and/or hydroxyls).

It is noteworthy that despite this reduction mechanism (similarly to chromate), the recycling of the sorbent is remarkably high compared to chromate case.

Table 4
XPS analysis of sorbent (before and after Se(VI) sorption, and after desorption) – Binding energies (BE, eV), atomic fractions (AF, %) and assignments.

Sample	A-PEI Membrane		A-PEI membrane after Se(VI) sorption		A-PEI membrane after Se(VI) desorption		Assignments
	BE (eV)	AF (%)	BE (eV)	AF (%)	BE (eV)	AF (%)	
C 1s	284.0	1.99	283.9	2.24	283.9	0.92	C—C
	284.6	88.7	284.7	90.3	284.5	86.1	C—C, C=C, C—H
	285.4	1.32	285.4	1.29	285.8	3.24	C—N
	287.1	8.02	287.2	6.17	287.1	9.77	C=N, C—O
N 1s	398.4	64.6	398.8	68.4	398.5	80.3	=N—
	399.7	3.60	—	—	400	18.4	—NH ₂
	400.8	31.8	400.7	31.6	401.5	1.3	—NH ₃ ⁺
O 1s	—	—	—	—	528.3	1.79	O ⁻
	529.8	8.20	529.6	9.40	529.9	7.82	C=O
	531.5	91.8	531.6	90.6	531.6	90.4	C—O
Se 3d	—	—	54.6	10.1	62.03	100	Se(-II)
	—	—	55.7	5.50	—	—	Se(0)
	—	—	58.69	84.4	—	—	Se(IV)

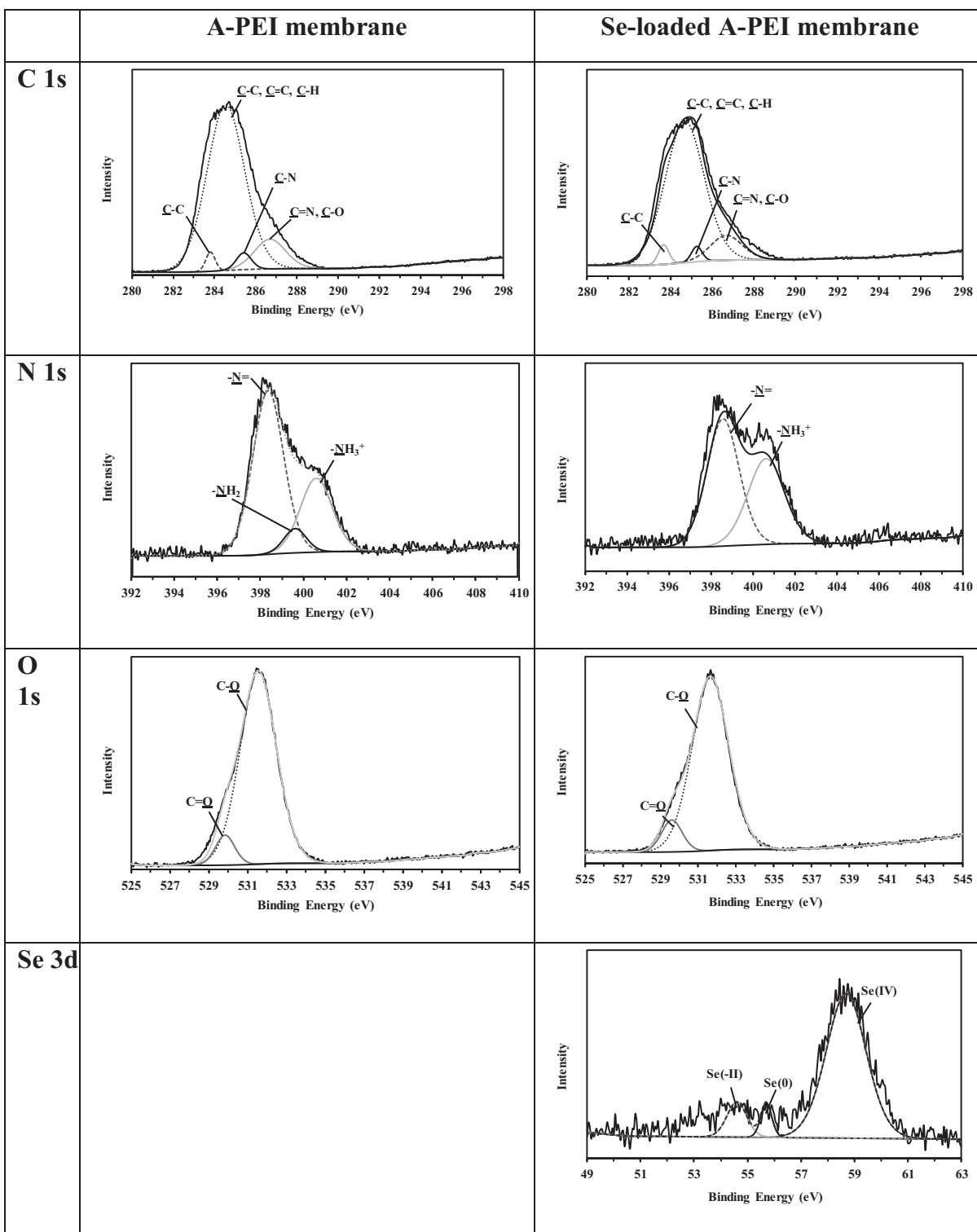


Fig. 7. High resolution C 1 s, O 1 s, N 1 s, and Se 3d core level XPS spectrum of A-PEI membrane and Se(VI)-loaded A-PEI membrane.

4. Conclusions

This work describes the readily synthesis of new highly percolating membranes (A-PEI membranes, prepared without sophisticated drying method) that are characterized by a great stability and strong affinity for selenate anions. Immobilized in fixed-bed column, fed with Se-containing solutions (under recirculation mode), A-PEI membranes show an optimum Se(VI) sorption at pH 2 due to strong affinity of protonated (primary) amine groups for anionic species. The sorption

isotherms are fitted by the Langmuir equation (better mathematical fit obtained with the 3-parameters equation of Sips): maximum sorption capacity at pH 2 reaches up to 83 mg g⁻¹. The flow rate (circulation mode) influences kinetic profiles at a superficial flow velocity below 2 m h⁻¹; above, the flow rate hardly changes the removal rate. The pseudo-first order rate equation fits well kinetic profiles, though the equilibrium sorption capacities calculated by the pseudo-second order rate equation are closer from experimental equilibrium values. Sulfate anions (with chemical properties very close to SeO₄²⁻) have a marked

effect on selenate binding contrary to chloride and nitrate anions. Selenium can be easily desorbed from loaded sorbent using 0.01 M NaOH solutions (consistently with pH impact on Se(VI) sorption). The sorbent shows remarkably stable performances for both sorption and desorption, for at least four cycles.

The FTIR and XPS analyses confirm the conclusions raised from experimental sorption results: selenate anionic species are bound to protonated primary amine groups (preferentially to secondary amine groups) through Coulombic attraction. However, XPS analysis confirms that selenate was completely reduced; this reduction mechanism is accompanied by the simultaneous oxidation of some organic compounds at the surface of the sorbent. Despite these modifications, the regenerated membranes show FTIR and XPS spectra very close to those of raw material. This is consistent with the high stability of the material in terms of sorption performances. A-PEI membranes are promising sorbents for the recovery of selenate from dilute effluents; the highly percolating properties make possible their use as natural draining reactive supports.

Acknowledgments

Y. Mo acknowledges the China Scholarship Council (CSC, Grant No. 201708450080) for providing PhD fellowship. Authors thank Jean-Claude Roux (IMT Mines Alès, C2MA) for his technical support for SEM and SEM-EDX analyses. Authors thank Mohammed F. Hamza (Nuclear Materials Authority, Egypt) for his technical support for XPS analyses.

Appendix A. Supplementary material

Supplementary data to this article can be found online at <https://doi.org/10.1016/j.ijbiomac.2019.10.055>.

References

- A.D. Lemly, Aquatic selenium pollution is a global environmental safety issue, *Ecotoxicol. Environ. Saf.* 59 (1) (2004) 44–56.
- S. Santos, G. Ungureanu, R. Boaventura, C. Botelho, Selenium contaminated waters: An overview of analytical methods, treatment options and recent advances in sorption methods, *Sci. Total Environ.* 521 (2015) 246–260.
- WHO, Guidelines for drinking-water quality, WHO 2017 Geneva, Switzerland.
- M. Tuzen, A. Sari, Biosorption of selenium from aqueous solution by green algae (*Cladophora hutchinsiae*) biomass: equilibrium, thermodynamic and kinetic studies, *Chem. Eng. J.* 158 (2) (2010) 200–206.
- Y. Nakamaru, K. Tagami, S. Uchida, Distribution coefficient of selenium in Japanese agricultural soils, *Chemosphere* 58 (10) (2005) 1347–1354.
- P. Gurunathan, S. Hari, S.B. Suseela, R. Sankararajan, A. Mukannan, Production, characterization and effectiveness of cellulose acetate functionalized ZnO nanocomposite adsorbent for the removal of Se (VI) ions from aqueous media, *Environ. Sci. Pollut. Res.* 26 (1) (2019) 528–543.
- J. Torres, V. Pintos, L. Gonzatto, S. Dominguez, C. Kremer, E. Kremer, Selenium chemical speciation in natural waters: protonation and complexation behavior of selenite and selenate in the presence of environmentally relevant cations, *Chem. Geol.* 288 (1–2) (2011) 32–38.
- Y. Fu, J. Wang, Q. Liu, H. Zeng, Water-dispersible magnetic nanoparticle-graphene oxide composites for selenium removal, *Carbon* 77 (2014) 710–721.
- H. Asiabi, Y. Yamini, M. Shamsayei, Highly selective and efficient removal of arsenic(V), chromium(VI) and selenium(VI) oxyanions by layered double hydroxide intercalated with zwitterionic glycine, *J. Hazard. Mater.* 339 (2017) 239–247.
- J.S. He, J.P. Chen, A comprehensive review on biosorption of heavy metals by algal biomass: materials, performances, chemistry, and modeling simulation tools, *Bioresour. Technol.* 160 (2014) 67–78.
- R.M. Moghazy, A. Labena, S. Husien, Eco-friendly complementary biosorption process of methylene blue using micro-sized dried biosorbents of two macro-algal species (*Ulva fasciata* and *Sargassum dentifolium*): full factorial design, equilibrium, and kinetic studies, *Int. J. Biol. Macromol.* 134 (2019) 330–343.
- D. Park, Y.S. Yun, J.M. Park, Reduction of hexavalent chromium with the brown seaweed *Ecklonki* biomass, *Environ. Sci. Technol.* 38 (18) (2004) 4860–4864.
- C. Bertagnolli, M.G.C. da Silva, E. Guibal, Chromium biosorption using the residue of alginate extraction from *Sargassum filipendula*, *Chem. Eng. J.* 237 (2014) 362–371.
- A. Sari, O.D. Uluozlu, M. Tuzen, Equilibrium, thermodynamic and kinetic investigations on biosorption of arsenic from aqueous solution by algae (*Maugeotia geniflexa*) biomass, *Chem. Eng. J.* 167 (1) (2011) 155–161.
- L. Nouri, Z. Bendjama, A.E. Hamitouche, S. Boumaza, F. Kaouah, M. Trari, R. Ladji, Optimization of a novel biocomposite synthesis (Amni Visnaga extraction waste/alginate) for Cd²⁺ biosorption, *Int. J. Biol. Macromol.* 80 (2015) 588–595.
- J.S. Yang, Y.J. Xie, W. He, Research progress on chemical modification of alginate: a review, *Carbohydr. Polym.* 84 (1) (2011) 33–39.
- I.P.S. Fernando, K.K.A. Sanjeeva, S.Y. Kim, J.S. Lee, Y.J. Jeon, Reduction of heavy metal (Pb²⁺) biosorption in zebrafish model using alginate acid purified from *Ecklonia cava* and two of its synthetic derivatives, *Int. J. Biol. Macromol.* 106 (2018) 330–337.
- A. García, M. Culebras, M.N. Collins, J.J. Leahy, Stability and rheological study of sodium carboxymethyl cellulose and alginate suspensions as binders for lithium ion batteries, *J. Appl. Polym. Sci.* 135 (17) (2018) 46217.
- S.Y. Wang, T. Vincent, C. Faur, E. Guibal, A comparison of palladium sorption using polyethyleneimine impregnated alginate-based and carrageenan-based algal beads, *Appl. Sci.* 8 (2) (2018).
- T. Andersen, J.E. Melvik, O. Gaserod, E. Alsberg, B.E. Christensen, Ionically gelled alginate foams: physical properties controlled by type, amount and source of gelling ions, *Carbohydr. Polym.* 99 (2014) 249–256.
- S.B. Deng, Y.P. Ting, Characterization of PEI-modified biomass and biosorption of Cu (II), Pb(II) and Ni(II), *Water Res.* 39 (10) (2005) 2167–2177.
- Y. Mo, S. Wang, T. Vincent, J. Desbrieres, C. Faur, E. Guibal, New highly-percolating alginate-PEI membranes for efficient recovery of chromium from aqueous solutions, *Carbohydr. Polym.* 225 (2019), 115177.
- M.R. Torres, A.P.A. Sousa, E. Filho, F. Dirce, J.P.A. Feitosa, R.C.M. de Paula, M.G.S. Lima, Extraction and physicochemical characterization of *Sargassum vulgare* alginate from Brazil, *Carbohydr. Res.* 342 (14) (2007) 2067–2074.
- M.V. Lopez-Ramon, F. Stoeckli, C. Moreno-Castilla, F. Carrasco-Marín, On the characterization of acidic and basic surface sites on carbons by various techniques, *Carbon* 37 (8) (1999) 1215–1221.
- P. Eisel, J. Yeh, R.K. Latvala, L.D. Shea, D.J. Mooney, Porous carriers for biomedical applications based on alginate hydrogels, *Biomaterials* 21 (19) (2000) 1921–1927.
- V. Jaiswal, S. Saxena, I. Kaur, P. Dubey, S. Nand, M. Naseem, S.B. Sing, P.K. Srivastava, S.K. Barik, Application of four novel fungal strains to remove arsenic from contaminated water in batch and column modes, *J. Hazard. Mater.* 356 (2018) 98–107.
- X.W. Li, X.H. Dai, J. Takahashi, N. Li, J.W. Jin, L.L. Dai, B. Dong, New insight into chemical changes of dissolved organic matter during anaerobic digestion of dewatered sewage sludge using EEM-PARAFAC and two-dimensional FTIR correlation spectroscopy, *Bioresour. Technol.* 159 (2014) 412–420.
- J.B. Linden, M. Larsson, S. Kaur, W.M. Skinner, S.J. Miklavcic, T. Nann, I.M. Kempson, M. Nyden, Polyethyleneimine for copper absorption II: kinetics, selectivity and efficiency from seawater, *RSC Adv.* 5 (64) (2015) 51883–51890.
- Q. Xiao, X.H. Gu, S. Tan, Drying process of sodium alginate films studied by two-dimensional correlation ATR-FTIR spectroscopy, *Food Chem.* 164 (2014) 179–184.
- D.W. Cho, B.H. Jeon, C.M. Chon, Y. Kim, F.W. Schwartz, E.S. Lee, H. Song, A novel chitosan/clay/magnetite composite for adsorption of Cu(II) and As(V), *Chem. Eng. J.* 200 (2012) 654–662.
- L. Ayed, K. Chaieb, A. Cheref, A. Bakhrouf, Biodegradation and decolorization of triphenylmethane dyes by *Staphylococcus epidermidis*, *Desalination* 260 (1–3) (2010) 137–146.
- A.B. Hegge, T. Andersen, J.E. Melvik, E. Bruzel, S. Kristensen, H.H. Tonnesen, Formulation and bacterial phototoxicity of curcumin loaded alginate foams for wound treatment applications: studies on curcumin and curcuminoids XLII, *J. Pharm. Sci.* 100 (1) (2011) 174–185.
- B.N. Dickhaus, R. Priefer, Determination of polyelectrolyte pK_a values using surface-to-air tension measurements, *Colloids Surf. A* 488 (2016) 15–19.
- S.I. Ishikawa, S. Sekine, N. Miura, K. Suyama, K. Arihara, M. Itoh, Removal of selenium and arsenic by animal biopolymers, *Biol. Trace Elem. Res.* 102 (1–3) (2004) 113–127.
- H.Y. Peng, N. Zhang, M. He, B.B. Chen, B. Hu, Simultaneous speciation analysis of inorganic arsenic, chromium and selenium in environmental waters by 3-(2-aminoethylamino) propyltrimethoxysilane modified multi-wall carbon nanotubes packed microcolumn solid phase extraction and ICP-MS, *Talanta* 131 (2015) 266–272.
- C.E. Rodriguez-Martinez, Z.I. Gonzalez-Acevedo, M.T. Olguin, H. Frias-Palos, Adsorption and desorption of selenium by two non-living biomasses of aquatic weeds at dynamic conditions, *Clean Technol. Environ. Policy* 18 (1) (2016) 33–44.
- J.P. Simonin, On the comparison of pseudo-first order and pseudo-second order rate laws in the modeling of adsorption kinetics, *Chem. Eng. J.* 300 (2016) 254–263.
- C. Vincent, A. Hertz, T. Vincent, Y. Barre, E. Guibal, Immobilization of inorganic ion-exchanger into biopolymer foams - application to cesium sorption, *Chem. Eng. J.* 236 (2014) 202–211.
- Y.S. Ho, G. McKay, Pseudo-second order model for sorption processes, *Process Biochem.* 34 (5) (1999) 451–465.
- D.R. Roberts, A.M. Scheidegger, D.L. Sparks, Kinetics of mixed Ni-Al precipitate formation on a soil clay fraction, *Environ. Sci. Technol.* 33 (21) (1999) 3749–3754.
- C. Tien, Adsorption Calculations and Modeling, Butterworth-Heinemann, Newton, MA, 1994.
- S. Sheshmani, A. Ashori, S. Hasanzadeh, Removal of Acid Orange 7 from aqueous solution using magnetic graphene/chitosan: a promising nano-adsorbent, *Int. J. Biol. Macromol.* 68 (2014) 218–224.
- M.M. Motta, B.B. Mamba, J.M. Thwala, T.A.M. Msagati, Preparation, characterization, and application of polypropylene-clinoptilolite composites for the selective adsorption of lead from aqueous media, *J. Colloid Interface Sci.* 359 (1) (2011) 210–219.
- T.W. Weber, R.K. Chakravorty, Pore and solid diffusion models for fixed-bed adsorbents, *AIChE J.* 20 (2) (1974) 228–238.

- [45] S. Showmick, S. Chakraborty, P. Mondal, W. Van Renterghem, S. Van den Berghe, G. Roman-Ross, D. Chatterjee, M. Iglesias, Montmorillonite-supported nanoscale zero-valent iron for removal of arsenic from aqueous solution: Kinetics and mechanism, *Chem. Eng. J.* 243 (2014) 14–23.
- [46] N. Gezer, M. Gulfen, A.O. Aydin, Adsorption of selenite and selenate ions onto thiourea-formaldehyde resin, *J. Appl. Polym. Sci.* 122 (2) (2011) 1134–1141.
- [47] Y. Wu, Y. Chi, H. Bai, G. Qian, Y. Cao, J. Zhou, Y. Xu, Q. Lu, Z.P. Xu, S. Qiao, Effective removal of selenate from aqueous solutions by the Friedel phase, *J. Hazard. Mater.* 176 (1–3) (2010) 193–198.
- [48] T. Nishimura, H. Hashimoto, M. Nakayama, Removal of selenium(VI) from aqueous solution with polyamine-type weakly basic ion exchange resin, *Sep. Sci. Technol.* 42 (14) (2007) 3155–3167.
- [49] S.L. Lo, T.Y. Chen, Adsorption of Se(IV) and Se(VI) on an iron-coated sand from water, *Chemosphere* 35 (5) (1997) 919–930.
- [50] L.V. Constantino, J.N. Quirino, A.M. Monteiro, T. Abrao, P.S. Parreira, A. Urbano, M.J. Santos, Sorption-desorption of selenite and selenate on Mg-Al layered double hydroxide in competition with nitrate, sulfate and phosphate, *Chemosphere* 181 (2017) 627–634.
- [51] H. Dong, Y. Chen, G. Sheng, J. Li, J. Cao, Z. Li, Y. Li, The roles of a pillared bentonite on enhancing Se(VI) removal by ZVI and the influence of co-existing solutes in groundwater, *J. Hazard. Mater.* 304 (2016) 306–312.
- [52] Z. Ma, C. Shan, J. Liang, M. Tong, Efficient adsorption of selenium(IV) from water by hematite modified magnetic nanoparticles, *Chemosphere* 193 (2018) 134–141.
- [53] J.S. Yamani, A.W. Lounsbury, J.B. Zimmerman, Adsorption of selenite and selenate by nanocrystalline aluminum oxide, neat and impregnated in chitosan beads, *Water Res.* 50 (2014) 373–381.
- [54] Y.T. Chan, Y.T. Liu, Y.M. Tzou, W.H. Kuan, R.R. Chang, M.K. Wang, Kinetics and equilibrium adsorption study of selenium oxyanions onto Al/Si and Fe/Si coprecipitates, *Chemosphere* 198 (2018) 59–67.
- [55] M. Min, C. Shen, L. Fang, B. Zhu, J. Li, L. Yao, Y. Jiang, C. Xiong, Design of a selective regenerable cellulose microcolumn for selenium efficient recovery and economic determination, *Chem. Eng. Res. Des.* 117 (2017) 773–783.
- [56] N.K. Asmel, A.R.M. Yusoff, S.K. Lakkaboyana, Z.A. Majid, S. Salmiati, High concentration arsenic removal from aqueous solution using nano-iron ion enrich material (NIEM) super adsorbent, *Chem. Eng. J.* 317 (2017) 343–355.
- [57] B. Chen, Z. Zhu, Y. Guo, Y. Qiu, J. Zhao, Facile synthesis of mesoporous Ce-Fe bimetal oxide and its enhanced adsorption of arsenate from aqueous solutions, *J. Colloid Interface Sci.* 398 (2013) 142–151.
- [58] C. Sellitti, J.L. Koenig, H. Ishida, Surface characterization of graphitized carbon-fibers by attenuated total reflection Fourier-transform infrared spectroscopy, *Carbon* 28 (1) (1990) 221–228.
- [59] D. Peak, D.L. Sparks, Mechanisms of selenate adsorption on iron oxides and hydroxides, *Environ. Sci. Technol.* 36 (7) (2002) 1460–1466.
- [60] N. Chubar, EXAFS and FTIR studies of selenite and selenate sorption by alkoxide-free sol-gel generated Mg-Al-CO₃ layered double hydroxide with very labile interlayer anions, *J. Mater. Chem. A* 2 (38) (2014) 15995–16007.
- [61] J. Ma, Y. Wang, L. Zhou, S. Zhang, Preparation and characterization of selenite substituted hydroxyapatite, *Mater. Sci. Eng., C* 33 (1) (2013) 440–445.
- [62] W. Zhang, Y. Chai, N. Cao, Y. Wang, Synthesis and characterization of selenium substituted hydroxyapatite via a hydrothermal procedure, *Mater. Lett.* 134 (2014) 123–125.
- [63] R.C. Elder, P.E. Ellis, Selenite complexes with pentaamminecobalt(III) - O-bound and Se-bound forms, *Inorg. Chem.* 17 (4) (1978) 870–874.
- [64] K. Baek, A. Ciblak, X. Mao, E.-J. Kim, A. Alshwabkeh, Iron anode mediated transformation of selenate in sand columns, *Water Res.* 47 (17) (2013) 6538–6545.
- [65] H. Zhou, Y. Wang, R. He, F. Yu, J. Sun, F. Wang, Y. Lan, Z. Ren, S. Chen, One-step synthesis of self-supported porous NiSe₂/Ni hybrid foam: an efficient 3D electrode for hydrogen evolution reaction, *Nano Energy* 20 (2016) 29–36.
- [66] J. You, C. Zhao, J. Cao, J. Zhou, L. Zhang, Fabrication of high-density silver nanoparticles on the surface of alginate microspheres for application in catalytic reaction, *J. Mater. Chem. A* 2 (22) (2014) 8491–8499.
- [67] M.F. Hamza, Y. Wei, H.I. Mira, A.A.H. Abdel-Rahman, E. Guibal, Synthesis and adsorption characteristics of grafted hydrazinyl amine magnetite-chitosan for Ni(II) and Pb(II) recovery, *Chem. Eng. J.* 362 (2019) 310–324.
- [68] Y. Chen, X. Yan, J. Zhao, H. Feng, P. Li, Z. Tong, Z. Yang, S. Li, J. Yang, S. Jin, Preparation of the chitosan/poly(glutamic acid)/alginate polyelectrolyte complexing hydrogel and study on its drug releasing property, *Carbohydr. Polym.* 191 (2018) 8–16.
- [69] E.I. El-Shafey, Sorption of Cd(II) and Se(IV) from aqueous solution using modified rice husk, *J. Hazard. Mater.* 147 (1–2) (2007) 546–555.
- [70] Y.-Z. Yan, Q.-D. An, Z.-Y. Xiao, S.-R. Zhai, B. Zhai, Z. Shi, Interior multi-cavity/surface engineering of alginate hydrogels with polyethylenimine for highly efficient chromium removal in batch and continuous aqueous systems, *J. Mater. Chem. A* 5 (32) (2017) 17073–17087.
- [71] B. Qiu, J. Guo, X. Zhang, D. Sun, H. Gu, Q. Wang, H. Wang, X. Wang, X. Zhang, B.L. Weeks, Z. Guo, S. Wei, Polyethylenimine facilitated ethyl cellulose for hexavalent chromium removal with a wide pH range, *ACS Appl. Mater. Interfaces* 6 (22) (2014) 19816–19824.
- [72] M. Szlachta, N. Chubar, The application of Fe-Mn hydrous oxides based adsorbent for removing selenium species from water, *Chem. Eng. J.* 217 (2013) 159–168.
- [73] R.-X. Zhou, J.-H. Zhao, Z.-M. Wei, Simulation and optimization of the selenium recovery process using the continuous counter-current decantation ion exchange system, *Chem. Eng. J.* 191 (2012) 386–393.
- [74] R. Kamaraj, S. Vasudevan, Decontamination of selenate from aqueous solution by oxidized multi-walled carbon nanotubes, *Powder Technol.* 274 (2015) 268–275.
- [75] Y.T. Chan, W.H. Kuan, T.Y. Chen, M.K. Wang, Adsorption mechanism of selenate and selenite on the binary oxide systems, *Water Res.* 43 (17) (2009) 4412–4420.
- [76] W. Cui, P. Li, Z. Wang, S. Zheng, Y. Zhang, Adsorption study of selenium ions from aqueous solutions using MgO nanosheets synthesized by ultrasonic method, *J. Hazard. Mater.* 341 (2018) 268–276.
- [77] M. Li, A. Dopilka, A.N. Kraetz, H. Jing, C.K. Chan, Layered double hydroxide/chitosan nanocomposite beads as sorbents for selenium oxoanions, *Ind. Eng. Chem. Res.* 57 (14) (2018) 4978–4987.
- [78] Y.N. Larimi, M.H. Mallah, M.A. Moosavian, J. Safdari, Kinetic and equilibrium study of selenium removal from wastewater in mag-molecular process, *Desalin. Water Treat.* 57 (2) (2016) 933–948.
- [79] N. Bleiman, Y.G. Mishael, Selenium removal from drinking water by adsorption to chitosan-clay composites and oxides: Batch and columns tests, *J. Hazard. Mater.* 183 (1–3) (2010) 590–595.